Bone Marrow Transplantation Augments the Effect of Brain- and Spinal Cord-Directed Adeno-Associated Virus 2/5 Gene Therapy by Altering Inflammation in the Murine Model of Globoid-Cell Leukodystrophy

Adarsh S. Reddy[1], **Joong H. Kim**[2], **Jacqueline A. Hawkins-Salsbury**[1], **Shannon L. Macauley**[1], **Elisabeth T. Tracy**[6], **Carole A. Vogler**[7], **Xialin Han**[8], **Sheng-Kwei Song**[2], **David F. Wozniak**[3], **Stephen C. Fowler**[9], **Robyn S. Klein**[1,4,5], and **Mark S. Sands**[1]

[1]Department of Internal Medicine, Washington University School of Medicine, St. Louis, Missouri 63110

[2]Department of Radiology, Washington University School of Medicine, St. Louis, Missouri 63110

[3]Department of Psychiatry, Washington University School of Medicine, St. Louis, Missouri 63110

[4]Department of Pathology and Immunology, Washington University School of Medicine, St. Louis, Missouri 63110

[5]Department of Anatomy and Neurobiology, Washington University School of Medicine, St. Louis, Missouri 63110

[6]Department of Surgery, Duke University Medical Center, Durham, North Carolina 27710

[7]Department of Pathology, Saint Louis University School of Medicine, St. Louis, Missouri 63104

[8]Diabetes and Obesity Research Center, Sanford-Burnham Medical Research Institute, Orlando, Florida 32827

[9]Department of Pharmacology and Toxicology, University of Kansas, Lawrence, Kansas 66045

Abstract

Globoid-cell leukodystrophy (GLD) is an inherited demyelinating disease caused by the deficiency of the lysosomal enzyme galactosylceramidase (GALC). A previous study in the murine model of GLD (twitcher) demonstrated a dramatic synergy between CNS-directed adeno-associated virus 2/5 (AAV2/5) gene therapy and myeloreductive bone marrow transplantation (BMT). However, the mechanism by which these two disparate therapeutic approaches synergize is not clear. In addition, the therapeutic efficacy may have been limited since the CNS-directed gene therapy was restricted to the forebrain and thalamus. In the current study, intrathecal and intracerebellar injections were added to the therapeutic regimen and the mechanism of synergy between BMT and gene therapy was determined. Although AAV2/5 alone provided supraphysiological levels of GALC activity and reduced psychosine levels in both the brain and spinal cord, it significantly increased CNS inflammation. Bone marrow transplantation alone

provided essentially no GALC activity to the CNS and did not reduce psychosine levels. When AAV2/5 is combined with BMT, there are sustained improvements in motor function and the median life span is increased to 123 d (range, 92–282 d) compared with 41 d in the untreated twitcher mice. Interestingly, addition of BMT virtually eliminates both the disease and AAV2/5-associated inflammatory response. These data suggest that the efficacy of AAV2/5-mediated gene therapy is limited by the associated inflammatory response and BMT synergizes with AAV2/5 by modulating inflammation.

Introduction

Globoid-cell leukodystrophy (GLD) (Krabbe's disease) is an autosomal recessive disease caused by a deficiency of the lysosomal enzyme galactosylceramidase (GALC). This leads to altered catabolism of galactosylceramide and an increase in the levels of a toxic glycolipid, psychosine (Suzuki et al., 2000). Psychosine accumulation is hypothesized to result in the death of the oligodendrocytes and leads to rapid demyelination (Suzuki, 1998). Clinical features include irritability, spasticity, seizures, and death typically by 2 years of age. The murine model (twitcher; GALC$^{-/-}$) recapitulates most aspects of the infantile form of the disease and has been an invaluable tool for the understanding of the pathogenesis and developing therapies for GLD (Kobayashi et al., 1980).

For GLD, the only currently available therapy is hematopoietic stem cell transplantation (HSCT) using either bone marrow (Krivit et al., 1998) or umbilical cord blood (Escolar et al., 2005). Although the exact therapeutic mechanism of HSCT is unknown, it is believed to involve GALC-positive donor-derived cells entering the CNS and cross-correcting the enzyme deficiency (Y. P. Wu et al., 2000).

It is known that therapy for GLD is most effective if initiated when the patients are presymptomatic, typically during the newborn period (Escolar et al., 2005). Unfortunately, HSCT in newborns is associated with a relatively high mortality rate (Weinberg, 2005). In addition, HSCT simply slows the progression of the disease (Escolar et al., 2005, 2006). This is consistent with preclinical experiments showing that bone marrow transplantation (BMT) performed at 9–10 d of age only increases the life span of the twitcher mice on the C57BL/6 background from 40 to ~80 d (Yeager et al., 1984). Hence, other therapies like gene therapy (Shen et al., 2002; Lin et al., 2005; Rafi et al., 2005), substrate reduction therapy (Biswas et al., 2003), and combination therapies (Biswas and LeVine, 2002; Lin et al., 2007; Galbiati et al., 2009) should be considered.

Gene therapy directed to the CNS in the neonatal twitcher mice resulted in supraphysiological levels of enzyme and was able to prolong the life span of the twitcher mice by only ~10–15 d (Lin et al., 2005; Rafi et al., 2005). Interestingly, when forebrain-directed adeno-associated virus 2/5 (AAV2/5) gene therapy is combined with myeloreductive BMT, a dramatic synergy is observed between both therapies (Lin et al., 2007). Unfortunately, the disease remains mostly uncorrected in the spinal cord and cerebellum. In the current study, myeloreductive BMT was combined with AAV2/5 gene delivery to forebrain, cerebellum, and spinal cord. Additional targeting of the cerebellum and spinal cord resulted in significant improvement in most outcome measures. The only exception was the tremor phenotype, which was not improved in animals receiving BMT.

To understand the mechanism of synergy, several inflammatory markers were qualitatively and quantitatively assessed. Despite providing essentially no enzyme activity and no decrease in psychosine, addition of BMT virtually eliminated the inflammation and greatly enhanced the effects of AAV2/5. These data strongly suggest that BMT when combined with AAV2/5 decreases inflammation, which provides the dramatic therapeutic synergy.

Materials and Methods

Animals

Heterozygous twitcher (GALC$^{+/-}$) mice on a congenic C57BL/6 background were obtained from The Jackson Laboratory. Mice were maintained under the supervision of M. S. Sands at Washington University School of Medicine. The mice were housed under standard conditions with *ad libitum* access to food and water. Homozygous twitcher mice (GALC$^{-/-}$) were obtained by heterozygous by heterozygous matings. The genotype was determined by twitcher-specific PCR (Sakai et al., 1996). Only the mice surviving until weaning were used for the study. All animal experiments were approved by the Institutional Animal Care and Use Committee at Washington University School of Medicine.

Recombinant AAV2/5 vector

The AAV2/5 vector used in this study has been previously described (Lin et al., 2005, 2007). The expression of murine GALC is under control of the chicken β-actin promoter and CMV enhancer. The 3′ end of the GALC cDNA has the 3′-untranslated region from the rabbit β-globin gene and SV40 poly(A) sequences. Adeno-associated virus 2 pseudotyped with the AAV 5 capsid (AAV2/5) was made at the University of Florida viral vector core using previously published methods (Zolotukhin et al., 1999). The AAV2/5 titer was determined by dot blot hybridization of DNase-resistant viral DNA and compared with known quantities of vector plasmid. The virus was diluted to a final titer of 1.3×10^{12} particles/ml and stored at $-70°$C until use.

Therapeutic regimen

The study consisted of the following groups: untreated wild type (untreated wt), untreated twitcher (untreated mut), BMT-only wild type (BMT-WT), BMT-only twitcher (BMT-mut), AAV2/5-only twitcher (AAV-mut), and combination-treated twitcher (AAV+BMT-mut).

The regimen for the AAV+BMT-mut group consisted of AAV2/5 injections on day 2 or 3 of life and BMT on the following day. Before injections, the newborn mice were anesthetized by inducing hypothermia on ice packs for 10–15 min. CNS-directed gene therapy consisted of an intrathecal injection (Elliger et al., 1999) and six intracranial injections. Injections were done into the neonatal spine in the midline at the upper lumbar vertebral column. A total of 20 μl of virus [15 μl of AAV2/5 and 5 μl of filter-sterilized 6% green food coloring (Durkee Products) in Ringer's lactate] was injected using a 50 μl Hamilton syringe (Hamilton Company). The procedure was considered successful only if the green dye reached the posterior fontanelle. For intracranial delivery, 2 μl of AAV2/5 was injected at each of six sites (three sites per hemisphere) into the brain. Injections were performed using a Hamilton syringe fitted with a 32 gauge needle based on the sutural landmarks visible in a day 2 neonatal mouse. The depth of injection was controlled by using a guard on the needle. The injection sites were as follows: (1) forebrain, 2 mm lateral and 1 mm caudal to bregma and 1.5 mm deep; (2) thalamus, 2 mm lateral and 2.5 mm caudal to bregma and 2.5 mm deep; and (3) cerebellum, 1 mm lateral and 3 mm posterior to lambda and 2.5 mm deep.

For BMT, the bone marrow donors were sex-matched syngenic WT (GALC$^{+/+}$) mice expressing GFP under the control of CAGGS promoter (Okabe et al., 1997). Newborn mice received 400 rad of total body gamma radiation from a ^{137}Cs source for conditioning followed by injection of 10^6 GFP$^+$ sex-matched unfractionated nucleated bone marrow cells in 100 μl volume into the superficial temporal vein (Sands and Barker, 1999).

Flow cytometry

To quantify the hematopoietic-derived cells in the CNS (Sedgwick et al., 1991; Campanella et al., 2002; Cardona et al., 2006; McCandless et al., 2006), perfused mice brains were treated with collagenase/DNase buffer after homogenization and passed through a 70 μm filter. The hematopoietic-derived cells were isolated by separation on Percoll gradient. Cells were then counted using a hemocytometer and stained with fluorophore-conjugated antibodies after Fc receptor block. The following cells were identified and quantified by flow cytometry: Resting microglia (CD11b^{hi}, CD45^{lo}), activated microglia/macrophages (CD11b^{hi}, CD45^{hi}), CD8 T-cells, CD4 T-cells and neutrophils (Gr1^{hi}, F4/80$^-$). Spleen and bone marrow from wild-type animals were used for positive controls. Data were acquired using CellQuest Pro software (BD Biosciences) and analyzed using FlowJo software (Tree Star). The absolute cell numbers isolated from each brain were calculated using the hemocytometer cell counts and the percentage of cells that are stained with a respective combination of fluorophores. For quantifying donor hematopoietic engraftment, bone marrow was harvested from femurs at 36 d of age and the percentage of GFP$^+$ cells were determined.

Quantitation of psychosine

Psychosine levels were quantified in the brains and spinal cords at postnatal day 36, essentially as described previously (Jiang et al., 2009). Briefly, tissues were flash-frozen, pulverized, and weighed. Internal standard *N,N*-dimethylpsychosine was added at this stage, and lipids were extracted with 2:1 chloroform/methanol containing 5% ammonium hydroxide. Extracted lipids were treated with 1.0 $_M$ lithium hydroxide in methanol, and then washed with diethylether and hexanes, and extracted with chloroform. Lipids were then dried under nitrogen and resuspended in 1:1 chloroform/methanol. This sample was analyzed by mass spectrometry as described previously (Jiang et al., 2009). Psychosine concentration was calculated by comparing the psychosine peak intensity to that of the internal standard.

Multiplex sandwich immunoassays

This assay is based on a procedure described by Hulse et al. (2004). The Bio-Plex multiplex cytokine kit (Bio-Rad Laboratories) was used for these analyses, and the assays were performed essentially as per the manufacturers' specifications. The following cytokines were quantified: IL-1α, IL-1β, IL-2, IL-3, IL-4, IL-5, IL-6, IL-9, IL-10, IL-12(p40), IL-12(p70), IL-13, IL-17, eotaxin, granulocyte colony-stimulating factor (G-CSF), granulocyte–macrophage colony-stimulating factor (GM-CSF), IFN-γ, keratinocyte chemoattractant (KC), macrophage chemoattractant protein 1 (MCP-1), macrophage-inflammatory protein 1α (MIP-1α), MIP-1β, regulated on activation normal T-cell expressed and secreted (RANTES), and TNF-α. PBS-perfused mice brains were homogenized in a solution consisting of 10 m$_M$ Tris (pH 7.5), 150 m$_M$ NaCl, 1 m$_M$ dithiothreitol, 0.2% Triton X-100, and 20 μl/ml protease inhibitor mixture (P8340; Sigma-Aldrich). The supernatant from brain homogenates was diluted to obtain a protein target concentration of 0.5–1.0 mg/ml and stored at −70°C. Once thawed, the supernatant from the homogenates was incubated with the fluorescent beads from the kit, washed, and then incubated with biotin-labeled antibody mixture. The samples were then incubated with streptavidin-PE and the fluorescence values were read and analyzed by the flow cytometry based Bio-Plex 2200 system (Bio-Rad Laboratories). The concentration of the cytokine in each sample was calculated by using the standard curve generated for each cytokine by the standards supplied in the kit.

Protein assay

Protein assays were performed to normalize cytokine levels, GALC activity and psychosine levels. Total protein concentration was determined using a protein assay reagent based on the Coomassie dye-binding assay (Bio-Rad). A standard curve was generated using known concentrations of BSA.

Immunohistochemistry

Brains and spinal cords were collected after the animals were perfused with PBS. The tissue was immersion fixed in 4% paraformaldehyde overnight at 4°C followed by cryoprotection in 30% sucrose at 4°C. The tissues were then frozen in Tissue-Tek OCT compound (Sakura Finetek) and cryosectioned. For immunostaining, the tissues were fixed in 4% paraformaldehyde for 30 min followed by peroxidase quenching with hydrogen peroxide for 15 min. The sections were then stained with the appropriate dilution of primary antibodies overnight at 4°C. The primary antibody was detected using the appropriate secondary antibody (1:1000 for streptavidin conjugated) using a Vectastain kit (PK-6101; Vector Laboratories) and developed using peroxidase kit (Vector Laboratories). The sections were then mounted, dehydrated, and coverslipped. The antibodies used were rabbit anti-mouse glial fibrillary acidic protein (GFAP) (1:200; Immunostar), rat anti-mouse CD68 (1:1000; AbD Serotec), anti-rabbit secondary from the Vectastain kit (PK-6101; Vector Laboratories), and mouse absorbed anti-rat secondary (Vector Laboratories).

GALC activity

Brains and spinal cords were flash frozen in liquid nitrogen after perfusion. They were then homogenized and the supernatant was frozen at −70°C until ready to use. GALC activity was determined by cleaving radioactively labeled ^{3}H-galactosylceramide (Wenger, 1991). Excess uncleaved substrate was extracted using chloroform/methanol saturated with galactose. The free ^{3}H-galactose activity was measured in a scintillation counter as counts per minute, and the specific activity of the enzyme was calculated as nanomoles of substrate cleaved per hour per milligram of total protein.

Histochemical staining for GALC activity was performed using the previously described method (Dolcetta et al., 2004). Brains and spinal cords were processed for histology as above. Sections on slides were incubated in citrate-phosphate (CP) buffer, pH 4.5, for 15 min. They were then transferred to a solution containing 5 mg/ml taurodeoxycholic acid and 5 mg/ml oleic acid in CP buffer for 15 min. They were then incubated for 2 h in a solution containing taurodeoxycholate, oleic acid, 5 m$_M$ potassium ferricyanide, 5 m$_M$ potassium ferrocyanide, and 2 mg/ml X-Gal (Gold Biotechnology) in CP buffer. Sections were counterstained with Nuclear Fast Red (Sigma-Aldrich), dehydrated, and coverslipped.

Histology

For Luxol fast blue and periodic acid–Schiff (LFB/PAS) staining, tissues were processed as above and embedded in paraffin. Tenmicrometer-thick sagittal sections of the brain and transverse sections of the spinal cord were stained using standard procedures (Lin et al., 2007).

Tremor monitoring

Quantitative analysis of tremor was performed using an ultrasensitive force-plate actometer essentially as described previously (A. S. Reddy, D. F. Wozniak, N. B. Farber, S. C. Fowler, and M. S. Sands, unpublished observations). The animals were acclimated for at least 30 min in the same room before tremor monitoring. Data recording was conducted between 2:00 P.M. and 6:00 P.M. Data were collected for 6 min, but only the first minute, when

movement was maximal, was used for the tremor analyses. Briefly, 12 bit integer raw data files were acquired with a LabMaster interface (Scientific Solutions) that was controlled by a DOS-based Free Pascal program (http://www.freepascal.org). Custom-written Free Pascal programs were used to calculate distance traveled and the number of low mobility bouts (see below).

The following data were extracted from the raw data files (Fowler et al., 2001): (1) Fz, the net force exerted by the animal. Each time series [Fz(t)] was Fourier transformed using the fft function in MATLAB (MathWorks). A 500 point Hanning time-domain data window was used. The individual frequencies obtained after Fourier transformation were plotted as a continuous function (power spectrum) after filtering to retain frequencies between 2.5 and 30.0 Hz. (2) The frequency at peak power was taken as the frequency at which the power was at its maximum. (3) Power between 13 and 20 Hz was obtained by integrating the area under the power spectrum curve between 13 and 20 Hz. The aforementioned power spectrum variables (1) to (3) were computed for each individual mouse, and these variables were then subjected to standard statistical treatments (see below).

Life span and behavioral testing

The life span was measured by noting the date of death or killing. Animals were humanely killed if they had hindlimb paralysis or appeared moribund. Body weight was measured weekly. Behavioral testing was performed using previously established protocols (Lin et al., 2007). Accelerating rotarod and wire hang tests were performed every 5 d starting at 25 d of age. In the accelerating rotarod (3–9 rpm), the maximum time for the animal to fall off the rotarod was noted. In the wire hang test, the latency of the animal to fall, from holding an inverted cage lid, was noted. The maximum latency for both the tests was 60 s, and the best value from three trials was used for analysis. An n of 10–15 were used per group. Repeated-measures analysis could not be performed because of attrition. ANOVA was performed instead at two predetermined time points (35 and 70 d).

Diffusion tensor imaging

Briefly, five 36-d-old animals from different treatment groups underwent diffusion tensor imaging (DTI), as described previously (Hofling et al., 2009), with isoflurane/oxygen anesthesia. Diffusion-weighted images were obtained using Stejskal–Tanner spin-echo diffusion-weighted sequence (Stejskal and Tanner, 1965) in an Oxford Instruments 200/330 magnet (4.7 T, 40 cm clear bore) equipped with a 10 cm inner diameter, actively shielded Magnex gradient coil (maximum strength, 60 G/cm; rise time, 200 ms). The magnet, gradient coil, and gradient power supply were interfaced with a Varian Unity INOVA console controlled by a Sun Blade 1500 work station (Sun Microsystems). Multiple transverse slices covering L1–L3 spinal cord levels were obtained with the following parameters: TR, 1500 ms (determined by the respiratory rate of the mouse); TE, 37 ms; slice thickness, 1.0 mm; field of view, 1 cm $\times$ 1 cm; data matrix, 128 $\times$ 128 (zero-filled to 256 $\times$ 256). Diffusion-sensitizing gradients were applied in six orientations: (Gx, Gy, Gz) = (E, E, 0), (E, 0, E), (0, E, E), ($-E, E$, 0), (0, $-E, E$), and (E,0, $-E$), where $E = 0.707$ with a gradient strength = 13.5 G/cm, gradient duration (δ) = 7 ms, and gradient separation (Δ) = 18 ms resulting in b values of 0 and 1000 s/mm^2. The diffusion tensor for each pixel was estimated using a weighted linear least-squares method (Koay et al., 2006). Eigenvalue decomposition was then applied to the tensor, yielding a set of eigenvalues ($\lambda 1$, $\lambda 2$, $\lambda 3$) and eventually axial diffusivity ($\lambda \| = \lambda 1$), and radial diffusivity [$\lambda \perp = (\lambda 2 + \lambda 3)/2$] diffusivity for each pixel. Regions of interest (ROIs) for dorsal spinal cord white matter (DWM) and ventrolateral spinal cord white matter (VLWM) were drawn using ImageJ software. The DTI parameters for each ROI were averaged across three spinal cord levels (L1–L3), including eight 1 mm consecutive slices.

Statistical methods

GraphPad Prism (GraphPad Software) and R (www.R-project.org) (R Development Core Team, 2009) software were used to generate graphs and perform statistical analysis. Survival curves were generated by Kaplan–Meier method, and analysis was done using log rank test. Multiple group comparisons were done using ANOVA and were followed by Bonferroni's multiple-comparison procedures. Analysis of behavioral data was done using one-way ANOVA at specific time points with *post hoc* Bonferroni's comparisons.

Results

GALC activity

To provide a sensitive test for evaluating conditions with decreased GALC activity, we conducted an ANOVA followed by pairwise comparisons on the untreated wt, untreated mut, and BMT-mut groups. A significant ANOVA ($p = 0.0048$) indicated that the groups differed in GALC activity. *Post hoc* comparisons showed that GALC activity in the untreated mut group was significantly less than that of the untreated wt group, and compared with the untreated mut group, there was no significant increase in GALC activity in the BMT-mut group (Fig. 1*A*). A similar ANOVA model was used to evaluate treatments that increased GALC activity and included untreated wt, AAV-mut, and AAV+BMT-mut groups. In the AAV-mut and AAV+BMT-mut groups, GALC activity was significantly different ($p < 0.0001$) and approximately fivefold greater than untreated wt levels. There was no significant difference between the AAV-mut and AAV+BMT-mut groups (Fig. 1*B*).

The distribution of enzyme activity in the brain and the spinal cord was evaluated using a histochemical stain for GALC (Dolcetta et al., 2004) (Fig. 1*C–N*). Galactosylceramidase activity in the forebrain is concentrated in the lateral ventricles in the AAV-mut and AAV +BMT-mut groups (asterisk) (Fig. 1*E,F*). There are also GALC-positive cells spread throughout the cortex and hippocampus. In the hindbrain, the enzyme activity is prominent in the ependyma of the fourth ventricle (Fig. 1*I,J*, asterisk). In the spinal cord, intense enzyme activity is seen in the meninges (Fig. 1*M,N*). There appears to be a spread of the activity along the initial part of the spinal nerve roots to the spinal gray matter (Fig. 1*M,N*, arrowheads).

Hematopoietic engraftment and donor-derived cells in the CNS

Hematopoietic chimerism and donor cell infiltration into the CNS were measured at 36 d of age using flow cytometry by determining the percentage of GFP$^+$ cells in the bone marrow and brain, respectively (Fig. 2). All groups receiving BMT had hematopoietic chimerism between 3 and 29%. There was no significant difference in the levels of bone marrow engraftment between the various groups receiving BMT (Fig. 2*A*). There was no significant increase in GFP$^+$ cells (FL1 channel) in the brains of animals receiving BMT compared with background fluorescence (Fig. 2*B*).

Psychosine levels

Psychosine is a toxic metabolite that is known to accumulate in the CNS of the twitcher mice (Igisu and Suzuki, 1984) and is used as a biochemical surrogate to assess efficacy of treatment (Ichioka et al., 1987). Statistical analyses similar to that performed for GALC activity were used to compare psychosine levels between different groups. Psychosine levels in the brain and the spinal cord (Fig. 3*A,C*) showed that the levels are significantly increased in the untreated mut group compared with the untreated wt group. In the brains and spinal cords of the AAV-mut and in AAV+BMT-mut groups (Fig. 3*B,D*), the levels of psychosine are significantly less than untreated twitcher mice and approach those of normal animals.

Interestingly, BMT alone does not reduce psychosine levels in either brain or spinal cord compared with untreated twitcher mice (Fig. 3*A,C*).

Histology: LFB and PAS

Brains and spinal cord of various treatment groups were examined for myelin architecture and globoid cells using LFB/PAS staining. The corpus callosum of the brains of untreated wt mice (Fig. 4*A*) showed extensive staining with LFB and no PAS-positive cells. Three 36-d-old untreated mut brains had numerous PAS-positive cells within the white matter (Fig. 4*B*, arrowheads). Occasional PAS-positive cells were also seen in the cortex. Two of the three mice in the AAV-mut group (Fig. 4*C*) and all three mice examined in the AAV+BMT-mut group (Fig. 4*D*) appeared to have a slight reduction in the number of PAS-positive macrophages in the white matter. Two of the three mice in the AAV+BMT-mut group also had cerebellar dysplasia with loss of the normal cerebellar architecture. The brains of the BMT-mut group animals were not examined.

There appeared to be a slight reduction in the number of PAS$^+$ cells in the spinal cords of all three animals from both the AAV-mut and AAV+BMT-mut groups (Fig. 4*G,H*). The three mice examined from the BMT-mut group failed to show any obvious reduction in the PAS-positive cells in the spinal cord (data not shown), and the sections appeared histologically indistinguishable from those seen in the untreated mut group (Fig. 4*F*).

DTI of the spinal cord

Using diffusion tensor imaging, axial diffusivity ($\lambda\|$) and radial diffusivity ($\lambda\perp$) were measured *in vivo* in the DWM and VLWM from all study groups. The radial and axial diffusivity heat maps are shown in Figure 5*A–H*. In the DWM, axial diffusivity of the untreated mut and the AAV-mut groups show a significant reduction compared with the untreated wt group (Fig. 5*I*). Interestingly, there is a significant increase in the axial diffusivity in the AAV+BMT-mut group compared with the untreated mut group (Fig. 5*I*). In the VLWM, a significant decrease in the axial diffusivity was observed in the untreated mut group compared with the untreated wt group (Fig. 5*J*). In both the AAV-mut and AAV+BMT-mut groups, $\lambda\|$ was comparable with that of the untreated wt group (Fig. 5*J*).

The *in vivo* radial diffusivity in the DWM of the untreated mut group (Fig. 5*K*) was significantly higher than that of the untreated wt group. There was no significant difference between the untreated wt group and the AAV-mut or AAV+BMT-mut groups. In the VLWM, a significant increase in radial diffusivity was seen in untreated mut mice relative to the untreated wt, AAV-mut, and AAV+BMT-mut groups (Fig. 5*L*).

Life span and behavior

Twitcher mice have a significantly shortened median life span (41 d) compared with normal littermates. There is a significant ($p < 0.001$) increase in median life span to 71 d (Fig. 6*A*) in the AAV-mut group. There is a further increase in the median life span to 123 d (range, 92–282 d) in animals from the AAV+BMT-mut group. The increase in median life span of the AAV+BMT-mut group compared with the AAV-mut group was highly significant ($p < 0.001$).

Untreated mut mice have significant behavioral deficits as measured by the rotarod and wire hang tests (Fig. 6*B,C*). At 35 d, the AAV-mut and AAV+BMT-mut groups performed significantly better than untreated mut mice on the accelerating rotarod. At 70 d of age, the AAV-mut and AAV+BMT-mut groups had significantly reduced latencies on the accelerated rotarod (Fig. 6*B*) compared with the untreated wt group. Interestingly, long-lived AAV+BMT-mut animals showed a sustained higher level of performance on the

rotarod until they were terminally ill. In contrast, the untreated mut and AAV-mut groups showed a steady decline in motor function as they aged. These observations suggest that hindlimb paralysis or weakness, which is prominent in the untreated mut group, appeared much less severe in the AAV+BMT-mut group.

The results from the wire hang test were consistent with these observations in that latencies to fall were significantly longer in the AAV+BMT-mut group compared with the untreated mut and the AAV-mut groups at the 35 d time point (Fig. 6*C*). There was no significant difference in performance between the AAV-mut group and the untreated mut group. At 70 d, the latency on the wire hang test was significantly higher in the AAV+BMT-mut group compared with the AAV-mut group, but the improvement was modest.

There is a significant increase in body weights in both the AAV-mut and AAV+BMT-mut groups at day 35 (Fig. 6*D*) compared with the untreated mut group. The animals in the AAV-mut group steadily lost weight beyond 40 d, whereas the animals in the AAV+BMT-mut group maintained their weight for the duration of the study.

Effect of treatment on tremor

Tremor is one of the characteristic phenotypes of the twitcher mouse. The effect of various treatments on the tremor phenotype was evaluated using a specially constructed force-plate actometer (Reddy, Wozniak, Farber, Fowler, and Sands, unpublished observations). The force variation created by the individual mice was analyzed after Fourier transformation of the raw data and the power spectra were generated from the output. The averaged power spectra of the untreated wt and AAV-mut groups appear similar (Fig. 7*A*). The untreated mut and AAV+BMT-mut groups appear similar to each other but different from the untreated wt and AAV-mut groups. Compared with the untreated wt group, the frequency of peak power and the power between 13 and 20 Hz were significantly increased in the AAV +BMT-mut group, but not in the AAV-mut group (Fig. 7*B,C*). There was no significant difference between the AAV-mut and AAV+BMT-mut groups with respect to the total distance traveled (Fig. 7*D*) or the number of low mobility bouts (data not shown). The similarities (i.e., nonsignificant differences) between the untreated wt and AAV-mut groups shown in Figure 7*A–D* collectively represent the therapeutic benefit of CNS-directed AAV2/ 5-mediated gene therapy on the tremor phenotype. The therapeutic benefit of CNS-directed AAV2/5- mediated gene therapy on tremor phenotype seemed to be negated with the addition of BMT.

To directly assess the effect of myeloreductive conditioning and BMT on tremor, the phenotype of wild-type mice that received BMT (BMT-WT) was assessed. The BMT-WT group had greater power in both the frequencies ~10–12 Hz and in the higher frequencies in the 13–20 Hz range compared with the untreated wt group (Fig. 7*A*). The power between 13 and 20 Hz (Fig. 7*C*) was significantly increased in the BMT-WT group compared with the untreated wt group. The total distance traveled was significantly decreased in the BMT-WT group compared with the untreated wt group (Fig. 7*D*).

CNS inflammation

CNS inflammation is a prominent pathologic feature of GLD. Numerous PAS-positive globoid cells (macrophages with engulfed myelin debris) are found in the white matter (Fig. 4) (Suzuki et al., 2000). Using flow cytometry, the various inflammatory cells in the brain were quantified (Fig. 8). Compared with the untreated wt group, the untreated mut group showed a trend toward an increase in $CD45^{hi}CD11b^+$ cells (activated microglia/ macrophages) (Fig. 8*B,F*). There is a significant increase in activated microglia/ macrophages, CD4 and CD8 T-cells in the AAV-mut group compared with the untreated wt

group (Fig. 8*A,C,D*). The presence of CD4 and CD8 T-cells was unique to the AAV-mut group. Interestingly, the increases in activated microglia, CD4 and CD8 T-cells were reversed in the AAV+BMT-mut group (Fig. 8*A–D,F*). There was no increase in neutrophil (Gr1^{hi}F4/80$^−$) numbers in any groups compared with the untreated wt group (data not shown).

Another important component of inflammation is the cytokines and chemokines. Several cytokines and chemokines were found to be altered in the brains of the twitcher mouse (Fig. 9). The most highly elevated cytokines in the untreated mut group compared with the untreated wt groups were KC (CXCL1) and IL-12(p40). Interestingly, KC and IL-12(p40) are significantly decreased ($p < 0.001$) in the AAV-mut and AAV+BMT-mut groups compared with the untreated mut group. There was a significant elevation in KC in the BMT-mut group compared with the untreated mut group. The cytokine MCP-1 was detected in the untreated mut and BMT-mut groups, but not in untreated wt, AAV-mut, or AAV +BMT-mut groups. The cytokines TNF-α and MIP-1β were decreased in the untreated mut group compared with the untreated wt group. The levels of these cytokines in the AAV-mut and AAV+BMT-mut groups were similar to that of the untreated wt group. Interestingly, no increase in these two cytokines was seen in the BMT-mut group.

The brains and spinal cords of the animals of various groups were immunostained for GFAP. Regions showing increased GFAP staining represent sites of active inflammation. GFAP staining was extensive in the brain and spinal cord of the untreated mut group (Fig. 10*B,F,J,N*). In the brains of the AAV-mut group (Fig. 10*C,G*), GFAP staining appeared to be similar or slightly decreased compared with that of the untreated mut group. However, in the brains of the AAV+BMT-mut group (Fig. 10 *D,H*), the staining was much less than either the untreated mut or the AAV-mut groups, although it seemed to be slightly more than that of the untreated wt group. In contrast, GFAP staining in the AAV-mut spinal cord seems to be similar to the AAV+BMT-mut group and much less than the untreated mut group (Fig. 10 *J–L*).

Similarly, when the brains and the spinal cords were immunostained for CD68 (macrosialin), increased immunoreactivity was seen in the untreated mut group (Fig. 11*B,F,J*) compared with the untreated wt group (Fig. 11*A,E,I*). In the AAV-mut group, the CD68 immunostaining was decreased in the forebrain and spinal cord (Fig. 11*C,J*) but appeared to be increased in the hindbrain. This correlates well with the overall similarity in the microglial number by flow cytometry (Fig. 8*F*). In the AAV+BMT-mut group, there appeared to be an overall decrease in CD68 immunostaining in the forebrain, cerebellum, and spinal cord compared with either untreated mut mice or AAV-mut mice (Fig. 11*D,H,L*).

Discussion

It is clear that no single therapy to date can completely treat GLD. Previous studies have shown that combining BMT with substrate reduction therapy, lentiviral-mediated or AAV2/5-mediated gene therapy resulted in additive or synergistic improvements (Biswas and LeVine, 2002; Lin et al., 2007; Galbiati et al., 2009). Combining BMT with AAV2/5 gene therapy (Lin et al., 2007) resulted in synergistic benefits. In the previous study (Lin et al., 2007), the AAV2/5-mediated gene therapy component was limited to the forebrain. Perhaps not surprisingly, there were no decreases in the disease markers in the cerebellum and spinal cord. In the current study, myeloreductive BMT was combined with AAV2/5-mediated gene therapy directed to the forebrain, cerebellum, and spinal cord. The increased gene delivery combined with BMT in the current study further improved motor function and increased life span. To our knowledge, this is the greatest clinical improvement observed in the twitcher mouse on the congenic C57BL/6 background. This improvement extended to

the cerebellum and spinal cord. Improved myelination was observed in the spinal cord as evidenced by decreased radial diffusivity on MRI. Radial diffusivity represents water diffusion perpendicular to the axon. When myelin damage occurs radial diffusivity increases (Hofling et al., 2009). Decreased axonal damage is also observed in the spinal cord as an increase in axial diffusivity. Axial diffusivity represents the water diffusion parallel to the axon. A decrease in axial diffusivity implies compromised axonal integrity (Hofling et al., 2009).

It has been hypothesized that the accumulation of psychosine in oligodendrocytes is the primary insult leading to the disease. It was recently shown that psychosine preferentially accumulates in lipid rafts and it was hypothesized that lipid raft perturbation is the cellular mechanism of psychosine toxicity (White et al., 2009). Both CNS-directed AAV2/5 gene therapy alone and in combination with BMT significantly reduced psychosine levels in the brain and spinal cord. It will be of interest to determine whether the distribution of psychosine is also altered following therapy.

Although nearly every clinical measure (life span, motor function, and body weight) was significantly improved in the animals receiving AAV+BMT compared with animals receiving AAV alone, the tremor was more severe in the combination-treated animals. This is clearly associated with the bone marrow transplant procedure and is most likely due to the conditioning radiation. We showed previously that conditioning radiation, even relatively low doses (200–400 rad), in neonatal animals causes cerebellar dysplasia (Sands et al., 1993). The CNS damage might be even worse with myeloablative conditioning regimens. These data demonstrate the benefits and drawbacks of BMT and highlight the need for less invasive treatments.

The combination therapy also dramatically decreased CNS inflammation. There is normalization of several cytokines, in particular IL-12(p40), KC (CXCL1), and MCP-1. Interestingly, the primary sources of these three cytokines in the brain are astrocytes and macrophages (Leonard and Yoshimura, 1990; Filipovic et al., 2003; Gee et al., 2009). The decrease in the above cytokines and chemokines correlates with the decreased number of macrophages and decreased astrocyte activation observed in the AAV-mut and AAV+BMT-mut groups, but not in the BMT-mut group.

The cytokine KC is increased in the untreated mut group compared with the untreated wt group. The primary role of KC is in neutrophil chemotaxis (Boisvert et al., 1998; Liu et al., 2010). Interestingly, there is no increase in neutrophil numbers in the brains of the untreated mut mice. However, KC is also known to affect oligodendrocyte proliferation and migration. Consistent with the actions of KC on oligodendrocytes, KC is elevated in demyelinating disease models like the jimpy mice (Q. Wu et al., 2000) and in brains of patients with multiple sclerosis (Filipovic et al., 2003). It is possible that the primary role of KC in GLD is to act as a chemoattractant and mitogen during oligodendrocyte development and/or repair (Tsai et al., 2002). The decrease in KC in the treated animals is consistent with reduced myelin damage.

The chemokine MCP-1 is a macrophage chemoattractant and is increased in the untreated mut and BMT-mut groups, both of which have greater numbers of histologically demonstrable globoid cells and increases in CD45^{hi}CD11b$^+$ cells by flow cytometry. The levels of the proinflammatory cytokines TNF-α and MIP-1β are decreased in the untreated mut group compared with the untreated wt group. Given the profound inflammatory response associated with GLD, one might predict that TNF-α would be increased. However, TNF-α signaling through TNF receptor 1 may not play a significant role in the progression of GLD. This is supported by the fact that the lack of TNF receptor 1 does not alter the

course of the disease in the twitcher mouse (Pedchenko et al., 2000). The reason for the decrease of TNF-α in the untreated mut group could be indicative of the profound and persistent demyelination associated with GLD. TNF receptor 2 is upregulated during demyelination and remyelination (Arnett et al., 2001) and may act as a sink effectively reducing TNF-α levels.

The current study clearly shows that CNS-directed AAV2/5-mediated gene therapy is associated with an increase in activated microglia, as well as CD4^{+} and CD8^{+} T-cells in the twitcher mouse. CD4 and CD8 T-cell responses are typically associated with viral infections (Doherty, 1985). An increase in CD4 and CD8 T-cells was also observed in normal control mice following an injection of the same vector expressing palmitoyl protein thioesterase 1, a ubiquitously expressed lysosomal enzyme (data not shown). Although AAV2/5-mediated gene therapy resulted in GALC levels severalfold higher than normal, the increased inflammatory response could contribute to the limited clinical improvements observed with this therapy alone. When BMT is added to the regimen, the AAV2/5-associated inflammation is virtually eliminated. This is especially interesting considering the fact that BMT alone provides little or no GALC activity, no decrease in psychosine, and seems to exacerbate certain aspects of the inflammatory response (KC, MCP-1, and IL-12). These data strongly support the hypothesis that BMT has a direct immunomodulatory effect on AAV2/5-mediated gene therapy and could explain the dramatic synergy. It also suggests that, in order for BMT to exert its immunomodulatory effects, GALC activity must also be present. The GALC activity is likely necessary to reduce psychosine levels, thus decreasing the toxic insult.

Although the immunomodulation by BMT seems to be a plausible explanation, there appears to be a discrepancy between the cellular inflammation and the cytokines. The AAV-mut group shows a decrease in some of the elevated cytokines but an increase in the cellular inflammation. However, the AAV+BMT-mut group shows a decrease in cytokine levels as well as a decrease in cellular inflammation. The cytokine elevations appear to correlate with the extent of demyelination rather than the infiltration of inflammatory cells.

In a different therapeutic paradigm, BMT using high-dose (800–900 rad) myeloablative radiation in 9- to 10-d-old mice is known to extend the life span in the twitcher mice (Yeager et al., 1984). Galactosylceramidase-positive bone marrow-derived cells have been shown to enter the CNS (Hoogerbrugge et al., 1988) and can result in GALC activity in the CNS as high as 15% of wild type (Hoogerbrugge et al., 1989). However, this level of enzyme results in an increase in median life span to only ~80 d (Yeager et al., 1984; Hoogerbrugge et al., 1989). Interestingly, a similar BMT regimen is also associated with downregulation of several proinflammatory cytokines in the twitcher mice (Y. P. Wu et al., 2001). Therefore, either decreasing inflammation or supplying enzyme, or both, appears to be responsible for the efficacy of BMT following high-dose conditioning. Based on the data presented here, we believe that immunomodulation plays a significant role in the efficacy of BMT. It will be particularly interesting to perform BMT experiments in the twitcher mice using conditions that allow for higher levels of engraftment during the neonatal period (Bruscia et al., 2006). This will help determine the respective contributions of enzyme activity and immunomodulation.

To summarize, myeloreductive BMT effectively augments the therapeutic benefit seen with CNS-directed AAV2/5-mediated gene therapy in GLD. Several reasons make the use of a myeloreductive conditioning regimen more attractive than the currently used myeloablative regimen. It is known that BMT is most effective when performed during the presymptomatic neonatal period and fully myeloablative neonatal BMT has a high mortality rate (Escolar et al., 2005; Weinberg, 2005). Myeloreductive conditioning regimens are known to result in

lower mortality, lower incidence of graft-versus-host disease, and stable engraftment (Jacobsohn et al., 2004; Shenoy et al., 2005). Therefore, we propose that combination therapy using an AAV vector and myeloreductive BMT during the neonatal period is a viable approach for treating GLD. Of course, this approach would be greatly facilitated by widespread implementation of newborn screening programs (Duffner et al., 2009). Future studies might further improve on this regimen by adding other therapies like substrate reduction (Young et al., 2004), increasing bone marrow engraftment, increasing the number of donor-derived cells entering the brain (Young et al., 2004), and using transduced bone marrow expressing high levels of enzyme (Naldini, 2011).

Acknowledgments

References

Arnett HA, Mason J, Marino M, Suzuki K, Matsushima GK, Ting JP. TNF alpha promotes proliferation of oligodendrocyte progenitors and remyelination. Nat Neurosci. 2001; 4:1116–1122. [PubMed: 11600888]

Biswas S, LeVine SM. Substrate-reduction therapy enhances the benefits of bone marrow transplantation in young mice with globoid cell leukodystrophy. Pediatr Res. 2002; 51:40–47. [PubMed: 11756638]

Biswas S, Biesiada H, Williams TD, LeVine SM. Substrate reduction intervention by l-cycloserine in twitcher mice (globoid cell leukodystrophy) on a B6;CAST/Ei background. Neurosci Lett. 2003; 347:33–36. [PubMed: 12865135]

Boisvert WA, Santiago R, Curtiss LK, Terkeltaub RA. A leukocyte homologue of the IL-8 receptor CXCR-2 mediates the accumulation of macrophages in atherosclerotic lesions of LDL receptor-deficient mice. J Clin Invest. 1998; 101:353–363. [PubMed: 9435307]

Bruscia EM, Ziegler EC, Price JE, Weiner S, Egan ME, Krause DS. Engraftment of donor-derived epithelial cells in multiple organs following bone marrow transplantation into newborn mice. Stem Cells. 2006; 24:2299–2308. [PubMed: 16794262]

Campanella M, Sciorati C, Tarozzo G, Beltramo M. Flow cytometric analysis of inflammatory cells in ischemic rat brain. Stroke. 2002; 33:586–592. [PubMed: 11823674]

Cardona AE, Huang D, Sasse ME, Ransohoff RM. Isolation of murine microglial cells for RNA analysis or flow cytometry. Nat Protoc. 2006; 1:1947–1951. [PubMed: 17487181]

Doherty PC. T cells and viral infections. Br Med Bull. 1985; 41:7–14. [PubMed: 3918607]

Dolcetta D, Perani L, Givogri MI, Galbiati F, Orlacchio A, Martino S, Roncarolo MG, Bongarzone E. Analysis of galactocerebrosidase activity in the mouse brain by a new histological staining method. J Neurosci Res. 2004; 77:462–464. [PubMed: 15248301]

Duffner PK, Caggana M, Orsini JJ, Wenger DA, Patterson MC, Crosley CJ, Kurtzberg J, Arnold GL, Escolar ML, Adams DJ, Andriola MR, Aron AM, Ciafaloni E, Djukic A, Erbe RW, Galvin-Parton P, Helton LE, Kolodny EH, Kosofsky BE, Kronn DF, et al. Newborn screening for Krabbe disease: the New York State model. Pediatr Neurol. 2009; 40:245–252. discussion 253–255. [PubMed: 19302934]

Elliger SS, Elliger CA, Aguilar CP, Raju NR, Watson GL. Elimination of lysosomal storage in brains of MPS VII mice treated by intrathecal administration of an adeno-associated virus vector. Gene Ther. 1999; 6:1175–1178. [PubMed: 10455422]

Escolar ML, Poe MD, Provenzale JM, Richards KC, Allison J, Wood S, Wenger DA, Pietryga D, Wall D, Champagne M, Morse R, Krivit W, Kurtzberg J. Transplantation of umbilical-cord blood in

babies with infantile Krabbe's disease. N Engl J Med. 2005; 352:2069–2081. [PubMed: 15901860]

Escolar ML, Poe MD, Martin HR, Kurtzberg J. A staging system for infantile Krabbe disease to predict outcome after unrelated umbilical cord blood transplantation. Pediatrics. 2006; 118:e879–e889. [PubMed: 16923928]

Filipovic R, Jakovcevski I, Zecevic N. GRO-alpha and CXCR2 in the human fetal brain and multiple sclerosis lesions. Dev Neurosci. 2003; 25:279–290. [PubMed: 12966224]

Fowler SC, Birkestrand BR, Chen R, Moss SJ, Vorontsova E, Wang G, Zarcone TJ. A force-plate actometer for quantitating rodent behaviors: illustrative data on locomotion, rotation, spatial patterning, stereotypies, and tremor. J Neurosci Methods. 2001; 107:107–124. [PubMed: 11389948]

Galbiati F, Givogri MI, Cantuti L, Rosas AL, Cao H, van Breemen R, Bongarzone ER. Combined hematopoietic and lentiviral gene-transfer therapies in newborn Twitcher mice reveal contemporaneous neurodegeneration and demyelination in Krabbe disease. J Neurosci Res. 2009; 87:1748–1759. [PubMed: 19185028]

Gee K, Guzzo C, Che Mat NF, Ma W, Kumar A. The IL-12 family of cytokines in infection, inflammation and autoimmune disorders. Inflamm Allergy Drug Targets. 2009; 8:40–52. [PubMed: 19275692]

Hofling AA, Kim JH, Fantz CR, Sands MS, Song SK. Diffusion tensor imaging detects axonal injury and demyelination in the spinal cord and cranial nerves of a murine model of globoid cell leukodystrophy. NMR Biomed. 2009; 22:1100–1106. [PubMed: 19650072]

Hoogerbrugge PM, Suzuki K, Suzuki K, Poorthuis BJ, Kobayashi T, Wagemaker G, van Bekkum DW. Donor-derived cells in the central nervous system of twitcher mice after bone marrow transplantation. Science. 1988; 239:1035–1038. [PubMed: 3278379]

Hoogerbrugge PM, Poorthuis BJ, Wagemaker G, van Bekkum DW, Suzuki K. Alleviation of neurologic symptoms after bone marrow transplantation in twitcher mice. Transplant Proc. 1989; 21:2980–2981. [PubMed: 2650408]

Hulse RE, Kunkler PE, Fedynyshyn JP, Kraig RP. Optimization of multiplexed bead-based cytokine immunoassays for rat serum and brain tissue. J Neurosci Methods. 2004; 136:87–98. [PubMed: 15126049]

Ichioka T, Kishimoto Y, Brennan S, Santos GW, Yeager AM. Hematopoietic cell transplantation in murine globoid cell leukodystrophy (the twitcher mouse): effects on levels of galactosylceramidase, psychosine, and galactocerebrosides. Proc Natl Acad Sci U S A. 1987; 84:4259–4263. [PubMed: 2884662]

Igisu H, Suzuki K. Progressive accumulation of toxic metabolite in a genetic leukodystrophy. Science. 1984; 224:753–755. [PubMed: 6719111]

Jacobsohn DA, Duerst R, Tse W, Kletzel M. Reduced intensity haemopoietic stem-cell transplantation for treatment of non-malignant diseases in children. Lancet. 2004; 364:156–162. [PubMed: 15246728]

Jiang X, Yang K, Han X. Direct quantitation of psychosine from alkaline-treated lipid extracts with a semi-synthetic internal standard. J Lipid Res. 2009; 50:162–172. [PubMed: 18753677]

Koay CG, Chang LC, Carew JD, Pierpaoli C, Basser PJ. A unifying theoretical and algorithmic framework for least squares methods of estimation in diffusion tensor imaging. J Magn Reson. 2006; 182:115–125. [PubMed: 16828568]

Kobayashi T, Yamanaka T, Jacobs JM, Teixeira F, Suzuki K. The Twitcher mouse: an enzymatically authentic model of human globoid cell leukodystrophy (Krabbe disease). Brain Res. 1980; 202:479–483. [PubMed: 7437911]

Krivit W, Shapiro EG, Peters C, Wagner JE, Cornu G, Kurtzberg J, Wenger DA, Kolodny EH, Vanier MT, Loes DJ, Dusenbery K, Lockman LA. Hematopoietic stem-cell transplantation in globoid-cell leukodystrophy. N Engl J Med. 1998; 338:1119–1126. [PubMed: 9545360]

Leonard EJ, Yoshimura T. Human monocyte chemoattractant protein-1 (MCP-1). Immunol Today. 1990; 11:97–101. [PubMed: 2186747]

Lin D, Fantz CR, Levy B, Rafi MA, Vogler C, Wenger DA, Sands MS. AAV2/5 vector expressing galactocerebrosidase ameliorates CNS disease in the murine model of globoid-cell leukodystrophy more efficiently than AAV2. Mol Ther. 2005; 12:422–430. [PubMed: 15996520]

Lin D, Donsante A, Macauley S, Levy B, Vogler C, Sands MS. Central nervous system-directed AAV2/5-mediated gene therapy synergizes with bone marrow transplantation in the murine model of globoid-cell leukodystrophy. Mol Ther. 2007; 15:44–52. [PubMed: 17164774]

Liu L, Belkadi A, Darnall L, Hu T, Drescher C, Cotleur AC, Padovani-Claudio D, He T, Choi K, Lane TE, Miller RH, Ransohoff RM. CXCR2-positive neutrophils are essential for cuprizone-induced demyelination: relevance to multiple sclerosis. Nat Neurosci. 2010; 13:319–326. [PubMed: 20154684]

McCandless EE, Wang Q, Woerner BM, Harper JM, Klein RS. CXCL12 limits inflammation by localizing mononuclear infiltrates to the perivascular space during experimental autoimmune encephalomyelitis. J Immunol. 2006; 177:8053–8064. [PubMed: 17114479]

Naldini L. Ex vivo gene transfer and correction for cell-based therapies. Nat Rev Genet. 2011; 12:301–315. [PubMed: 21445084]

Okabe M, Ikawa M, Kominami K, Nakanishi T, Nishimune Y. "Green mice" as a source of ubiquitous green cells. FEBS Lett. 1997; 407:313–319. [PubMed: 9175875]

Pedchenko TV, Bronshteyn IG, LeVine SM. TNF-receptor 1 deficiency fails to alter the clinical and pathological course in mice with globoid cell leukodystrophy (twitcher mice) but affords protection following LPS challenge. J Neuroimmunol. 2000; 110:186–194. [PubMed: 11024549]

Rafi MA, Zhi Rao H, Passini MA, Curtis M, Vanier MT, Zaka M, Luzi P, Wolfe JH, Wenger DA. AAV-mediated expression of galactocerebrosidase in brain results in attenuated symptoms and extended life span in murine models of globoid cell leukodystrophy. Mol Ther. 2005; 11:734–744. [PubMed: 15851012]

R Development Core Team. R: a language and environment for statistical computing. Vienna: R Foundation for Statistical Computing; 2009.

Sakai N, Inui K, Tatsumi N, Fukushima H, Nishigaki T, Taniike M, Nishimoto J, Tsukamoto H, Yanagihara I, Ozono K, Okada S. Molecular cloning and expression of cDNA for murine galactocerebrosidase and mutation analysis of the twitcher mouse, a model of Krabbe's disease. J Neurochem. 1996; 66:1118–1124. [PubMed: 8769874]

Sands MS, Barker JE. Percutaneous intravenous injection in neonatal mice. Lab Anim Sci. 1999; 49:328–330. [PubMed: 10403452]

Sands MS, Barker JE, Vogler C, Levy B, Gwynn B, Galvin N, Sly WS, Birkenmeier EH. Treatment of murine mucopolysaccharidosis type VII by syngeneic bone marrow transplantation in neonates. Lab Invest. 1993; 68:676–686. [PubMed: 8515654]

Sedgwick JD, Schwender S, Imrich H, Dörries R, Butcher GW, ter Meulen V. Isolation and direct characterization of resident microglial cells from the normal and inflamed central nervous system. Proc Natl Acad Sci U S A. 1991; 88:7438–7442. [PubMed: 1651506]

Shen JS, Watabe K, Meng XL, Ida H, Ohashi T, Eto Y. Establishment and characterization of spontaneously immortalized Schwann cells from murine model of globoid cell leukodystrophy (twitcher). J Neurosci Res. 2002; 68:588–594. [PubMed: 12111848]

Shenoy S, Grossman WJ, DiPersio J, Yu LC, Wilson D, Barnes YJ, Mohanakumar T, Rao A, Hayashi RJ. A novel reduced-intensity stem cell transplant regimen for nonmalignant disorders. Bone Marrow Transplant. 2005; 35:345–352. [PubMed: 15592491]

Stejskal EO, Tanner JE. Spin diffusion measurements: spin echoes in the presence of a time-dependent field gradient. J Chem Phys. 1965; 42:288.

Suzuki K. Twenty-five years of the "psychosine hypothesis": a personal perspective of its history and present status. Neurochem Res. 1998; 23:251–259. [PubMed: 9482237]

Suzuki, K.; Suzuki, Y.; Suzuki, K.; Wenger, DA. Metabolic and molecular bases of inherited diseases. New York: McGraw-Hill Professional; 2000. Galactosylceramide lipidosis: globoid cell leukodystrophy (Krabbe disease).

Tsai HH, Frost E, To V, Robinson S, Ffrench-Constant C, Geertman R, Ransohoff RM, Miller RH. The chemokine receptor CXCR2 controls positioning of oligodendrocyte precursors in developing spinal cord by arresting their migration. Cell. 2002; 110:373–383. [PubMed: 12176324]

Weinberg KI. Early use of drastic therapy. N Engl J Med. 2005; 352:2124–2126. [PubMed: 15901868]

Wenger, D. Techniques in diagnostic human biochemical genetics. New York: Wiley; 1991. Screening for lysosomal disorders; p. 587-617.

White AB, Givogri MI, Lopez-Rosas A, Cao H, van Breemen R, Thinakaran G, Bongarzone ER. Psychosine accumulates in membrane microdomains in the brain of Krabbe patients, disrupting the raft architecture. J Neurosci. 2009; 29:6068–6077. [PubMed: 19439584]

Wu Q, Miller RH, Ransohoff RM, Robinson S, Bu J, Nishiyama A. Elevated levels of the chemokine GRO-1 correlate with elevated oligodendrocyte progenitor proliferation in the jimpy mutant. J Neurosci. 2000; 20:2609–2617. [PubMed: 10729341]

Wu YP, McMahon E, Kraine MR, Tisch R, Meyers A, Frelinger J, Matsushima GK, Suzuki K. Distribution and characterization of GFP$^+$ donor hematogenous cells in Twitcher mice after bone marrow transplantation. Am J Pathol. 2000; 156:1849–1854. [PubMed: 10854208]

Wu YP, McMahon EJ, Matsuda J, Suzuki K, Matsushima GK, Suzuki K. Expression of immune-related molecules is downregulated in twitcher mice following bone marrow transplantation. J Neuropathol Exp Neurol. 2001; 60:1062–1074. [PubMed: 11706936]

Yeager AM, Brennan S, Tiffany C, Moser HW, Santos GW. Prolonged survival and remyelination after hematopoietic cell transplantation in the twitcher mouse. Science. 1984; 225:1052–1054. [PubMed: 6382609]

Young PP, Fantz CR, Sands MS. VEGF disrupts the neonatal blood-brain barrier and increases life span after non-ablative BMT in a murine model of congenital neurodegeneration caused by a lysosomal enzyme deficiency. Exp Neurol. 2004; 188:104–114. [PubMed: 15191807]

Zolotukhin S, Byrne BJ, Mason E, Zolotukhin I, Potter M, Chesnut K, Summerford C, Samulski RJ, Muzyczka N. Recombinant adeno-associated virus purification using novel methods improves infectious titer and yield. Gene Ther. 1999; 6:973–985. [PubMed: 10455399]
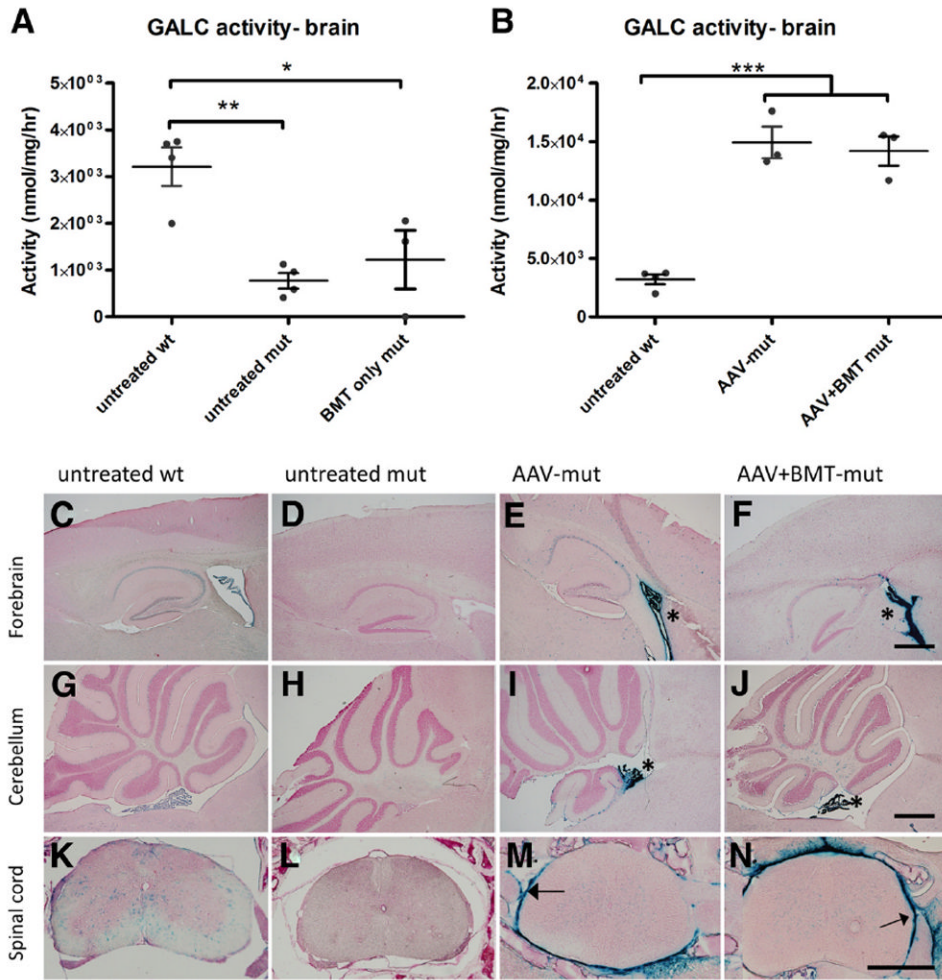
Figure 1.
GALC activity and distribution. GALC activity was significantly higher in the untreated wt mice compared with the untreated mut and BMT-mut groups (**A**). There was no significant difference between the untreated mutant and BMT-mut groups (**A**). A separate analysis showed that the GALC activity in the brains of AAV-mut and AAV+BMT-mut groups was approximately fivefold greater and significantly different from that of the untreated wt group (**B**). The horizontal bars represent means, and error bars represent SEM. $*p < 0.05$; $**p < 0.01$; $***p < 0.001$. GALC activity can be seen histochemically in the forebrain (**C**), cerebellum (**G**), and spinal cord (**K**) of the untreated wt group. In contrast, no GALC staining is observed in the forebrain (**D**), cerebellum (**H**), or spinal cord (**L**) of the untreated mut group. Intense GALC staining is observed in the ependyma of lateral and fourth ventricles of the AAV-mut and AAV+BMT-mut groups (asterisks; **E, F, I, J**). Intense staining was also observed in the meninges of the spinal cord and along the spinal nerve roots (arrows; **M, N**) of AAV-mut and AAV+BMT-mut mice. **C–J** were imaged at the same magnification. Scale bars: **F, J**, ~600 μm. **K–N** were imaged at the same magnification. Scale bar: **N**, ~600 μm.
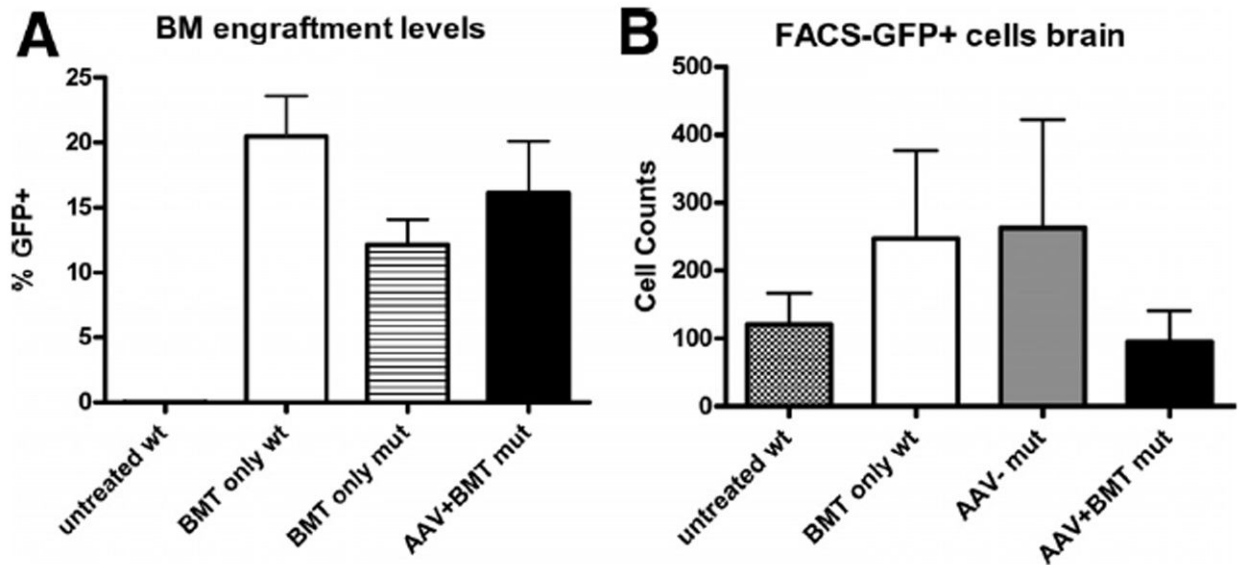
Figure 2.
Engraftment and GFP⁺ cells in the brain. The number of GFP⁺ donor cells present in the bone marrow and brains were determined using flow cytometry. The levels of bone marrow engraftment at day 36 were between 3 and 29%. There is no significant difference in donor engraftment in various groups receiving BMT (*A*). The number of cells present in FL1 channel ("GFP channel") in the brain was similar in all the groups tested. There is no significant difference in the GFP⁺ cells in the brains between the treated and untreated groups (*B*). Error bars indicate SEM.
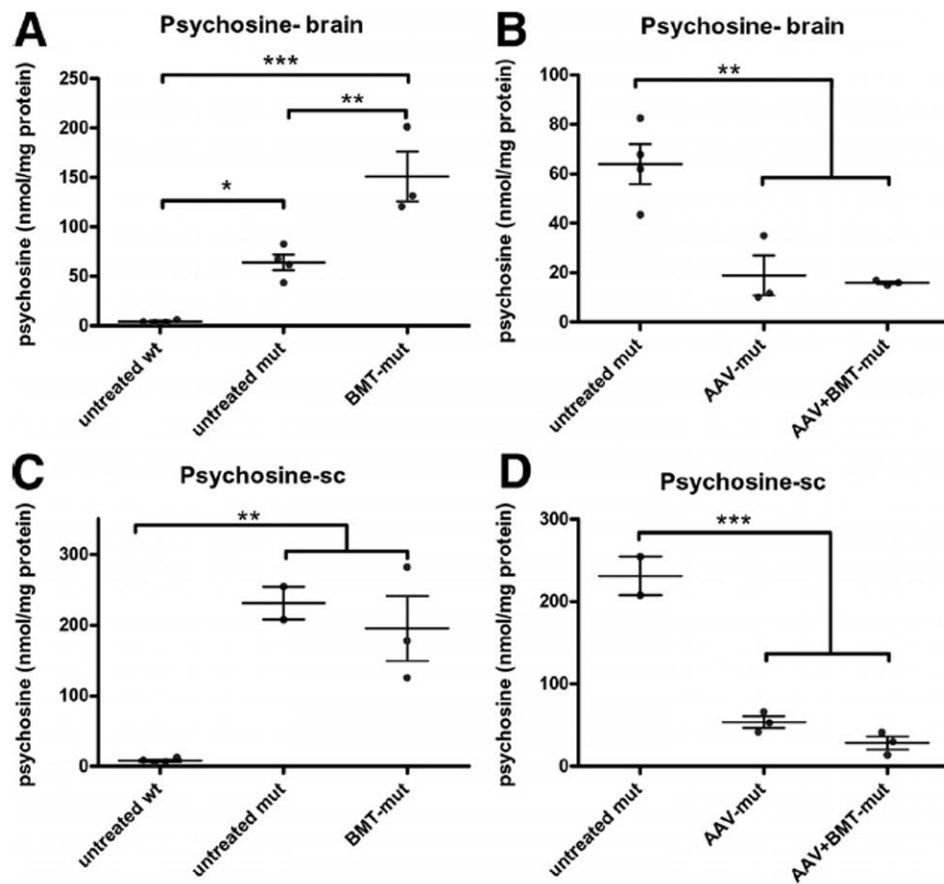
Figure 3.
Psychosine levels. Psychosine levels in the brain (Psychosine-brain; *A, B*) and the spinal cord (Psychosine-sc; *C, D*) were measured using mass spectrometry. In the brain, the psychosine levels were highly elevated in the untreated mut compared with untreated wt group, while levels were significantly increased in the BMT-mut group relative to both the untreated wt and untreated mut groups (*A*). In spinal cord, both the untreated mut and BMT-mut groups had significantly increased psychosine levels compared with the untreated wt mice (*C*). The analyses conducted on treatments that decreased psychosine levels showed that both the AAV-mut and AAV+BMT-mut groups had significantly reduced levels of psychosine compared with the untreated mut mice in both brain (*B*) and spinal cord (*D*). There was no significant difference in psychosine levels between the AAV-mut and AAV +BMT-mut groups in either the brains or spinal cord. The horizontal bars represent the means, and the error bars represent SEM. *$p < 0.05$; **$p < 0.01$; ***$p < 0.001$.

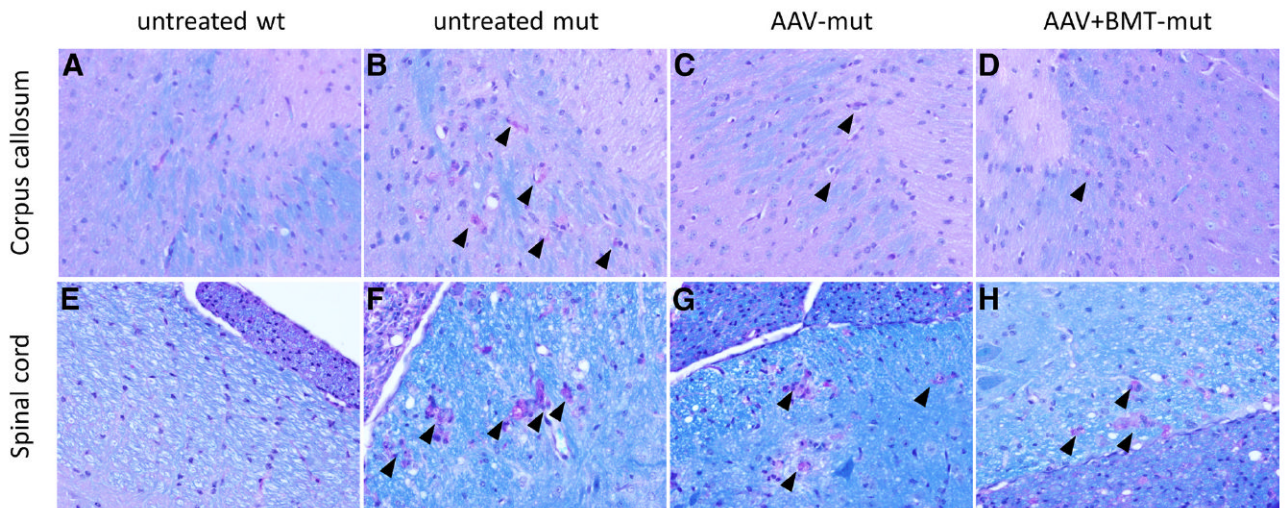**Figure 4.**
LFB-PAS. Luxol fast blue/periodic acid–Schiff staining of the anterior commissure of the corpus callosum of representative animals is shown (*A–D*). The untreated wt animal (*A*) has essentially no PAS-positive macrophages within the white matter, the untreated mut (*B*) mouse shows prominent PAS-positive macrophages within the white matter (arrowheads), and both the AAV-mut (*C*) and AAV+BMT-mut (*D*) mice show a reduction in the number of PAS-positive macrophages in this region of the brain. Sections from the lateral white matter of the spinal cord from an untreated wt mouse (*E*) show no PAS-positive macrophages within the white matter, whereas sections from the same area of an untreated 36-d-old twitcher mouse (*F*) show numerous PAS-positive macrophages (arrowheads). There appears to be a slight reduction of PAS-positive cells in the spinal cords of both the AAV-mut (*G*) and AAV+BMT-mut groups (*H*).
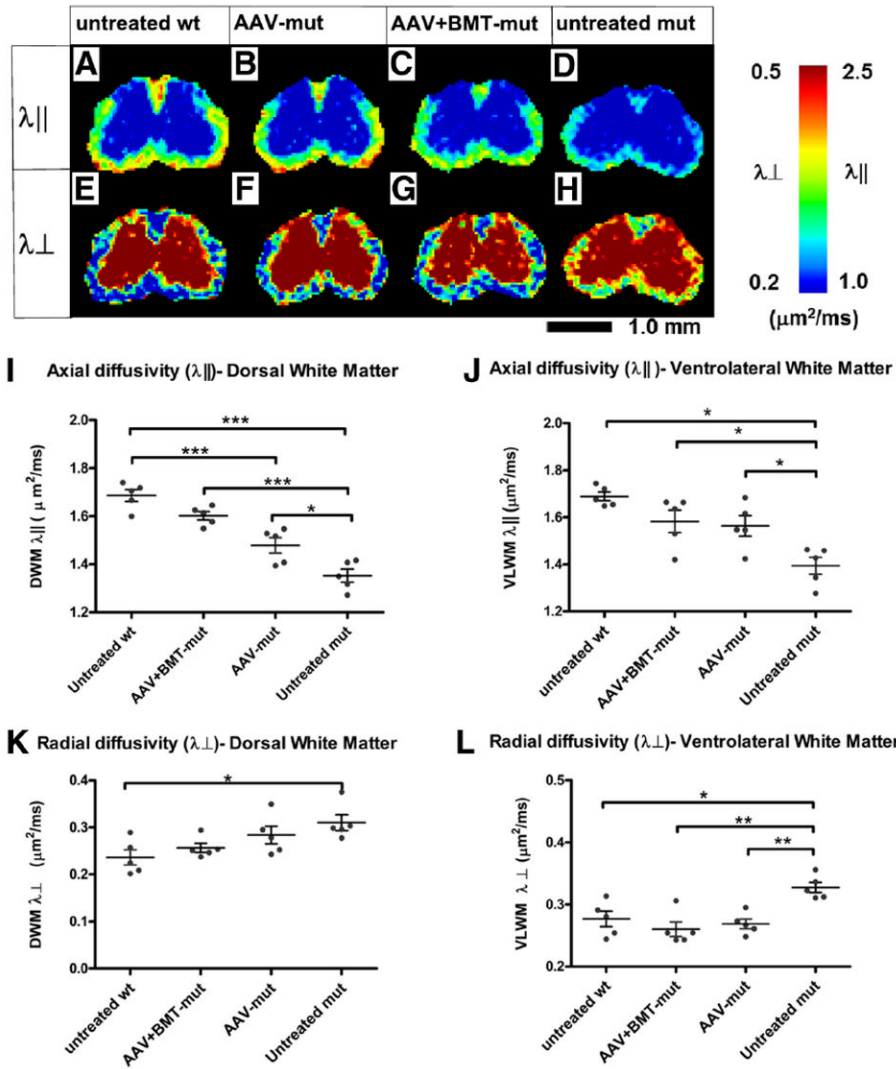
Figure 5.
Diffusion tensor imaging. Heat maps of axial diffusivity ($\lambda\parallel$; ***A–D***) and radial diffusivity ($\lambda\perp$; ***E–H***) in the spinal cord obtained by DTI. In the DWM (***I***), there is a significant decrease in the axial diffusion in the untreated mut group compared with the untreated wt group. The AAV-mut and AAV+BMT-mut groups show an increase in axial diffusion compared with the untreated mut group. In the VLWM (***J***), the axial diffusivity of the untreated mut is significantly decreased compared with the untreated wt and the treated groups. Radial diffusivity in the DWM (***K***) is significantly increased in the untreated mut compared with the untreated wt. The treated groups are intermediate between the untreated wt and untreated mut groups. In the VLWM (***L***), there is a significant increase in the radial diffusivity in the untreated mut compared with untreated wt. There is no significant difference between the untreated wt and the AAV-mut and AAV+BMT-mut groups. The horizontal bars represent the means, and the error bars represent SEM. *$p < 0.05$; **$p < 0.01$; ***$p < 0.001$; ns, not significant.
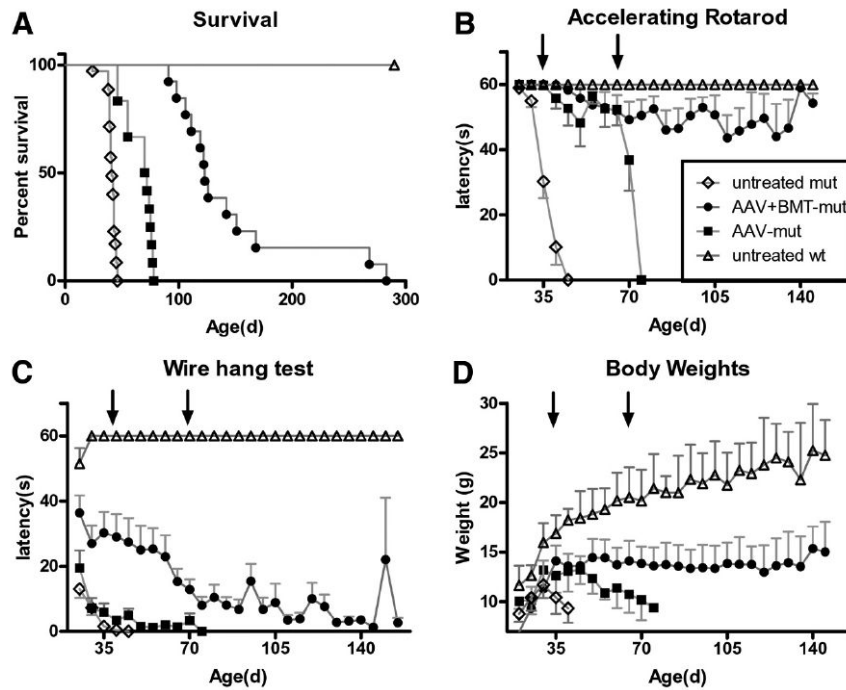
Figure 6.
Survival and behavior. Kaplan–Meier curves showing the survival of various treatment groups (*A*). The median life span of the AAV-mut group (71 d; range, 46 –78 d) was significantly greater than ($p < 0.001$) that of the untreated mut group (41 d; range, 24 – 46 d). The median life span of the AAV+BMT-mut group (123 d; range, 92–282 d) was significantly greater than that of the AAV-mut group ($p < 0.001$). Behavior was evaluated using constant speed rotarod and wire hang test. Animals in the AAV-mut and AAV+BMT-mut group performed significantly better than the untreated mut group in the accelerating (*B*) rotarod motor function tests at 35 d and at 70 d of age (arrows). There was a statistically significant improvement in latency on wire hang test only in the AAV+BMT-mut group (*C*) at day 35 of age. Body weights (*D*) in the AAV+BMT-mut group were significantly higher compared with the untreated mut at 35 d of age. There was no significant difference between the AAV-mut and untreated mut groups at 35 d of age. At 70 d of age, the body weights were significantly higher in the AAV+BMT-mut group compared with the AAV-mut group. The body weights were maintained in the long-lived animals from the AAV+BMT-mut group. Error bars represent SEM.
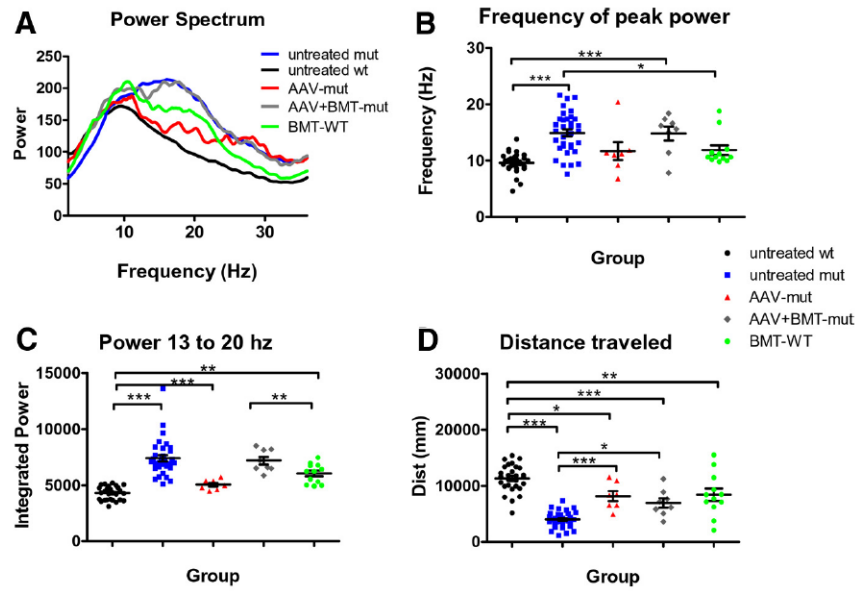
Figure 7.
Tremor. The averaged power spectrum (*A*) of the untreated mut group (blue line) is shifted toward higher frequencies with a broader bandwidth compared with the untreated wt group (solid black line). In the AAV-mut group (red line), the averaged power spectrum is similar to that of the untreated wild type. In the AAV+BMT-mut group (solid gray line), the power spectrum is shifted toward higher frequencies compared with the AAV-mut group and is similar to the untreated mut group. Compared with the untreated wt group, there is a significant increase in the frequency of peak power (*B*) and the power between 13 and 20 Hz (*C*) in the AAV+BMT-mut group, but not the AAV-mut group. The distance traveled by the AAV-mut and AAV+BMT-mut groups (*D*) is significantly increased compared with the untreated mut group. BMT alone altered the tremor phenotype in the wild-type mouse. The averaged power spectrum (*A*) of the BMT-WT group (solid green line) is shifted upward and rightward compared with the untreated wt group (solid black line). The frequency of peak power (*B*) and the power between 13 and 20 Hz (*C*) were significantly increased in the BMT-WT group compared with the untreated wild-type group. The distance traveled by the BMT-WT group was significantly decreased compared with the untreated wt group (*D*). The horizontal bars represent the mean, and the error bars represent SEM. ***$p < 0.001$; **$p < 0.01$; *$p < 0.05$.
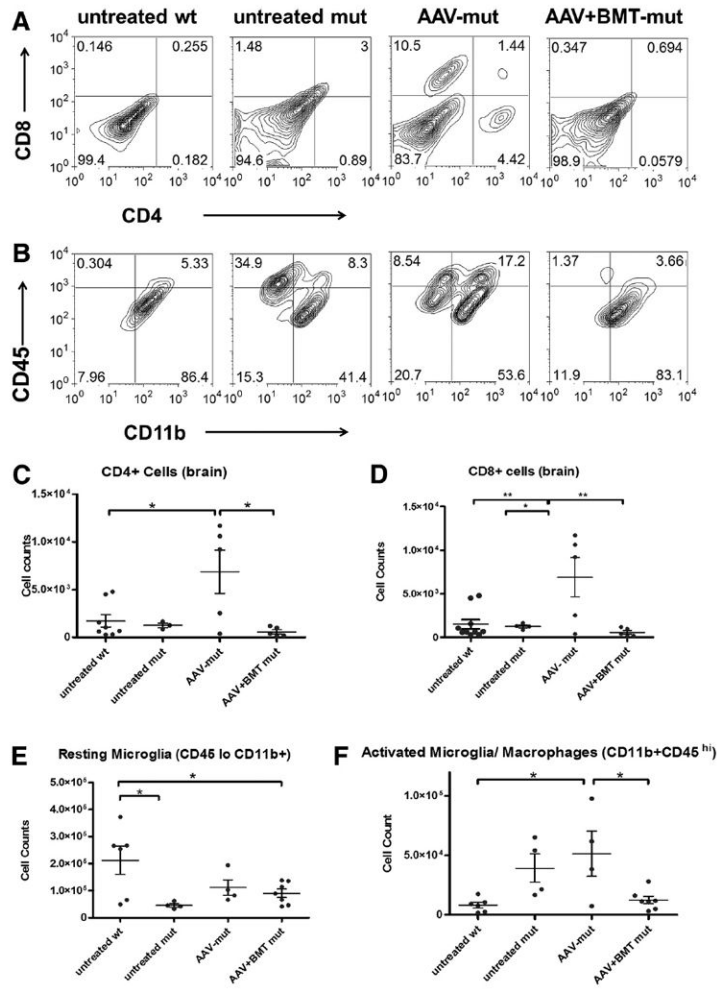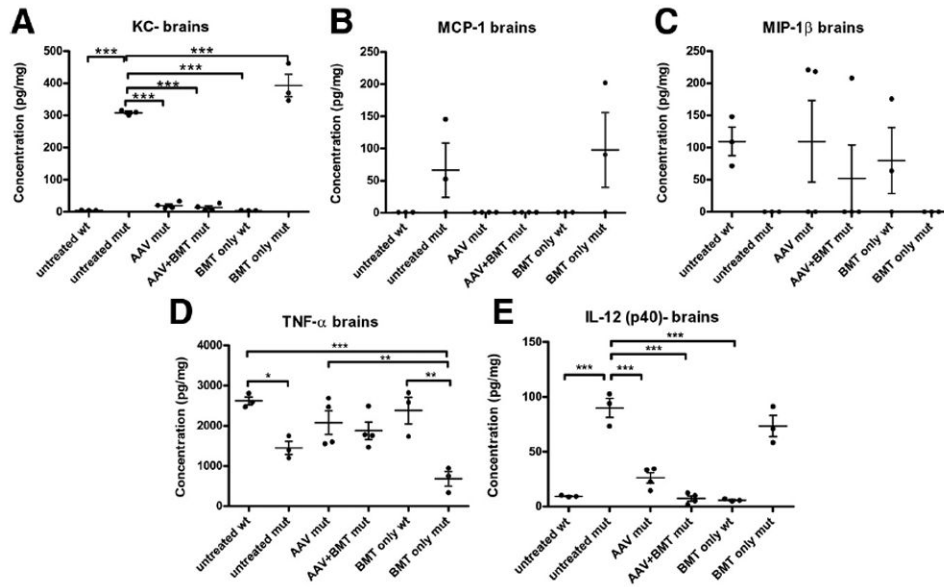
Figure 8.
Flow cytometry: brains. Representative bivariate plots show the relative numbers of CD4$^+$ and CD8$^+$ T-cells (*A*) and activated microglia (CD45 ^{hi}CD11b ^{hi}) (*B*) in brains of untreated wt, untreated mut, AAV-mut, and AAV+BMT-mut groups. Quantitation of T-cells shows that there is a significant increase in CD4 and CD8 T-cells (*C, D*) in the AAV-mut group compared with the untreated wt. There is no increase in CD4 and CD8 T-cells in the untreated mut and AAV+BMT-mut groups compared with the untreated wt group (*B–D*). There appears to be an increase in CD4, CD8, and activated microglia (CD45 ^{hi}CD11b ^{hi}) in the AAV-mut group compared with other groups. Quantitation of resting microglia (CD45 ^{lo}CD11b ^{hi}) (*E*) shows that there is a significant decrease in these cell numbers in the untreated mut and AAV+BMT-mut groups compared with the untreated wt group. Quantitation of activated microglia (*F*) shows that there is a significant increase in these cell numbers in the AAV-mut group compared with the untreated wt or AAV+BMT-mut group. There is no significant difference between the activated microglial numbers between untreated wt and AAV+BMT-mut groups. The horizontal bars represent means, and the error bars represent SEM. *$p < 0.05$, **$p < 0.01$.

Figure 9.
Chemokines and cytokines. There is a significant increase in KC (*A*) in the brains of the untreated mut animals compared with the untreated wt animals. The chemokine MCP-1 (***B***) is increased in the untreated mut group and is undetectable in the untreated wt group. In both the AAV-mut and AAV+BMT-mut groups, KC and MCP-1 levels are reduced similar to the untreated wt group. The BMT-mut group does not show a decrease in the above chemokines compared with the untreated mut group. The chemokine MIP-1β (***C***) is undetectable in the untreated mut group and is present in the AAV-mut and AAV+BMT-mut groups at levels comparable with the untreated wt group. The levels of MIP-1β in the BMT-mut group are similar to that of the untreated mut group. The cytokine TNF-α (***D***) is significantly decreased in the untreated mut group compared with the untreated wt group. In the AAV-mut and AAV+BMT-mut groups, the levels of TNF-α are similar to that of the untreated wt group. The levels of TNF-α in the BMT-mut group are similar to that of the untreated mut group. The cytokine IL-12(p40) (***E***) shows a trend similar to KC, with a significant increase in the untreated mut group compared with the untreated wt group. Levels of IL-12(p40) in the AAV-mut and AAV+BMT-mut groups are similar to the untreated wt group. The horizontal bars represent mean, and error bars represent SEM. *$p < 0.05$; **$p < 0.01$; ***$p < 0.001$; ns, not significant.
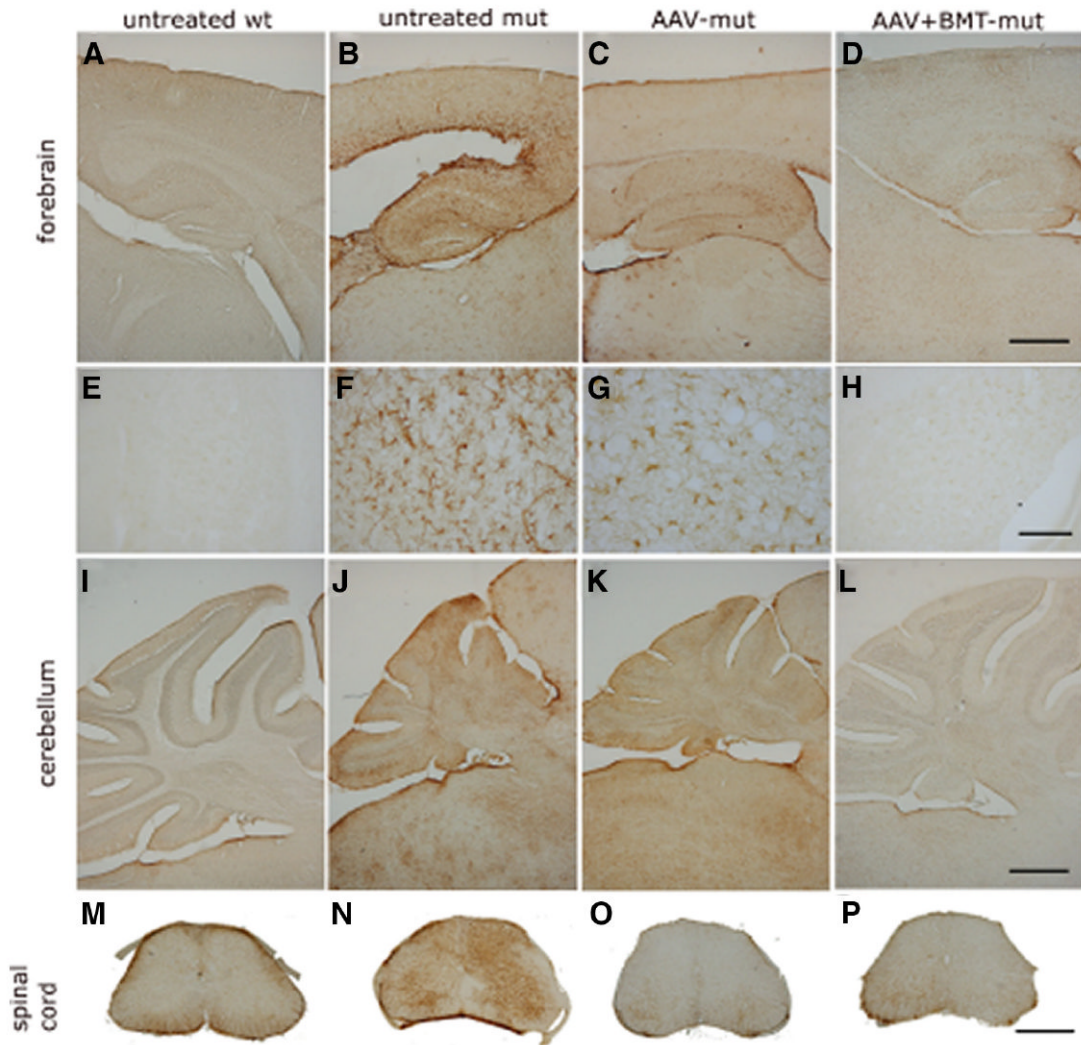
Figure 10.
GFAP immunohistochemistry. Representative images of GFAP staining of brain and spinal cords are shown. Untreated mut animals have higher GFAP immunoreactivity in all the regions of the CNS (*B, F, J, N*) compared with untreated wt animals (*A, E, I, M*). Animals in the AAV-mut group (*C, G, K, O*) appear to have similar or slightly decreased GFAP staining compared with the untreated mut group. The AAV+BMT-mut group (*D, H, L, P*) has less intense GFAP staining compared with the untreated mut and AAV-mut groups. High-magnification images (*E–H*) from the cortex show a characteristic activated astrocyte morphology. The spinal cords of the untreated wt group have minimal GFAP staining (*M*) compared with the untreated mut group (*N*). The spinal cords of the AAV-mut (*O*) and AAV +BMT-mut (*P*) groups stain with similar intensity as that of the untreated wt group. *A–D* and *I–P* were imaged at same magnification. Scale bars: *D, L, P*, ~600 μm. *E–H* were imaged at same magnification. Scale bar: *H*, ~25 μm.
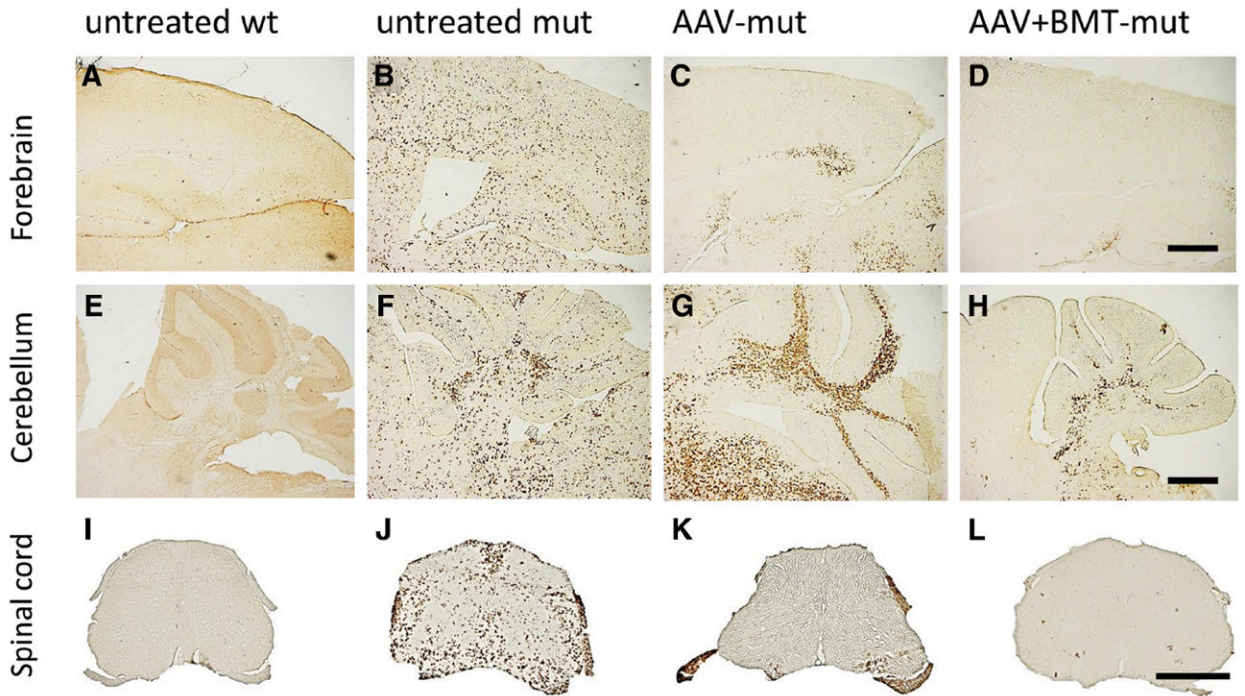
Figure 11.
CD68 immunohistochemistry. CD68 staining of the forebrain (*A–D*), cerebellum (*E–H*), and the spinal cord (*I–L*) at 36 d of age show increased staining in the untreated mut group (*B, F, J*). In the AAV-mut cerebellum (*G*), the CD68 staining appears similar or increased in intensity to that of the untreated mut (*F*). Interestingly, there appears to be decreased staining in the spinal cord (*K*) and the forebrain (*C*). In the AAV+BMT-mut group, the CD68 staining is decreased in most regions and indistinguishable from untreated wt mice in certain regions. *A–H* were imaged at the same magnification. Scale bars: *D, H*, ~600 μm. *I–L* were imaged at the same magnification. Scale bar: *L*, ~600 μm.